Lithium Perchlorate as a Solid/Liquid State Oxygen Source for Molecular Beam Epitaxy

A Thesis
Presented to
The Academic Faculty

by

Marshall Brooks Tellekamp Jr.

In Partial Fulfillment
of the Requirements for the Degree
Masters of Science in the
School of Electrical and Computer Engineering

Georgia Institute of Technology
August 2015

LITHIUM PERCHLORATE AS A SOLID/LIQUID STATE OXYGEN SOURCE FOR MOLECULAR BEAM EPITAXY

Approved by:

Dr. W. Alan Doolittle, Advisor
School of Electrical and Computer Engineering
Georgia Institute of Technology

Dr. William D. Hunt
School of Electrical and Computer Engineering
Georgia Institute of Technology

Dr. Paul Douglas Yoder
School of Electrical and Computer Engineering
Georgia Institute of Technology

Date Approved: 07/22/2015

To my wife, Page

ACKNOWLEDGEMENTS

I wish to thank Dr. Alan Doolittle for the hours of support and discussion which have enabled the completion of this work. I would like to thank Dr. Hunt and Dr. Yoder for agreeing to committee this thesis, as well as the support I have received from both of them in and out of the classroom. I also wish to thank my fellow researchers whose comments, critiques, and assistance have made this work possible, specifically Dr. Jordan Greenlee, Joshua Shank, Brendan Gunning, Chloe Fabien, Joseph Merola, and Evan Clinton. There would not be anyone to thank were it not for the constant unwavering support of my friends and my family, especially my mother, for which I am forever grateful. Finally I wish to thank my wife, Page, for always supporting my endeavors, even when I do not, and for pretending to enjoy science enough to listen to me gab on about it…I love you.

TABLE OF CONTENTS

LIST OF TABLES

LIST OF FIGURES

LIST OF SYMBOLS AND ABBREVIATIONS

T_c	Superconducting Critical Temperature (K)
E×N(E)	Energy specific Auger intensity N(E) multiplied by energy E
KLL	Auger transition levels (Core hole, relaxing electron, emitted electron)
I_0	Final Auger peak height
τ	Oxidation time constant
A	Fitting constant for Equation 4, or Amperes
m/q	Mass to charge ratio
2θ-ω	XRD diffraction angle for symmetric scans
Q_f	Quality Factor

AES	Auger Electron Spectroscopy
BCC	Body-Centered Cubic
BEP	Beam Equivalent Pressure
FCC	Face-Centered Cubic
FWHM	Full Width at Half Maximum
LTCC	Low Temperature Co-fired Ceramic
MBE	Molecular Beam Epitaxy
MIT	Metal-Insulator Transition
PBN	Pyrolytic Boron Nitride
RHEED	Reflection High Energy Electron Diffraction
SCCM	Standard Cubic Centimeter per Minute
SIMS	Secondary Ion Mass Spectrometry
UHV	Ultra-High Vaccuum
XRD	X-Ray Diffraction

SUMMARY

In order to grow metastable transition metal suboxides, $LiClO_4$ is theorized, designed, and tested as an alternative oxygen source for molecular beam epitaxy growth of oxide films. The material is found to decompose into a gas of both molecular and atomic oxygen beginning at approximately 250 °C, with an Arrhenius vapor pressure relationship across the measured range of less than 400 °C to avoid exothermic decomposition. A method for analyzing reaction rates is demonstrated using *in situ* Auger Electron Spectroscopy, and $LiClO_4$ is compared to O_2 showing a comparable reaction rate at four times lower growth pressure indicating the possibility for higher growth rates than are possible with O_2. The decomposition kinetics of $LiClO_4$ are discussed and solutions to instabilities are hypothesized for future studies on the material.

A new style of MBE effusion cell for the evaporation of high vapor pressure sources is also presented, utilizing a two-zone heating system and aperture plate to resolve radiative heating issues common to materials evaporated close to room temperature. Discussion follows the design and testing of the cell, which exhibits acceptable long term stability over a 3 week testing period.

These two sources are used, along with lithium, to grow thin films of multiple niobium oxidation states, from pure BCC niobium to $LiNbO_3$. The most important films are high quality $LiNbO_2$ which are grown using a method outlined in this work. The growth space is studied showing the preferential nucleation and growth of $LiNbO_2$ at 950 – 1000 °C and a lithium flux of approximately 3×10^{-7} torr beam equivalent pressure.

CHAPTER 1

INTRODUCTION

1.1 Motivation

Transition metal oxides have enabled and improved many technologies such as hydrogen production, methane production, photocatalysis, resistive ram, and memristors [1-3]. Often novel material properties are made possible by the d-orbital electrons found in transition metals such as niobium, which allow for various bonding mechanisms and oxidation states. In particular, several stable niobium oxides exist with different niobium to oxygen ratios due to the various niobium oxidation states. Niobium, as a transition metal, can oxidize alone as a +2, +4, and +5 valence forming the compounds NbO, NbO_2, and Nb_2O_5 [4-6]. Introducing lithium into these films allows three more fully oxidized (+5 valence) films, Li_3NbO_4, $LiNb_3O_8$, and $LiNbO_3$, as well as a suboxide (+3 valence) $LiNbO_2$. Of these materials NbO_2, Nb_2O_5, $LiNbO_3$, and $LiNbO_2$ are of particular interest for their variety of properties and applications in modern technology. NbO_2, the +4 suboxide, has been of recent interest as a Mott Memristor for neuromorphic applications as a neuristor and as a coupled oscillator due to the higher temperature metal insulator transition (MIT) at 1081 K [5, 7, 8]. Nb_2O_5 is a high-k dielectric for capacitors and is used to electroform NbO_2 [7]. $LiNbO_3$, which has piezoelectric and ferroelectric properties, is an important part of existing optics technology as waveguides, field activated wave plates (Pockels cell), surface acoustic wave devices, and second harmonic generators among other uses [9]. Li_xNbO_2 is a radiation hard [10] multifunctional material with resistive and optical properties tuned via lithium intercalation [11-17] and low T_c superconducting properties [18-21], as well as applications as a battery cathode

material [21-23]. An example of the wide range of properties demonstrated in the Li-Nb-O material system is shown in Figure 1 where the resistivity of various niobium and lithium niobium oxides is plotted as a function of niobium oxidation state.

Many properties such as ferromagnetism, piezoelectricity, and pyroelectricity rely on single crystalline material of the highest quality in order to maximize their effect, and many multi-functional devices have been realized by perovskite materials, heterojunctions, and superlattices such as $BiFeO_3$ and $BiTiO_3/SrTiO_3$ [24, 25]. It is therefore desirable to develop a method for growing high quality metal oxide films of varying metal oxidation state to exploit these multi-functional properties.

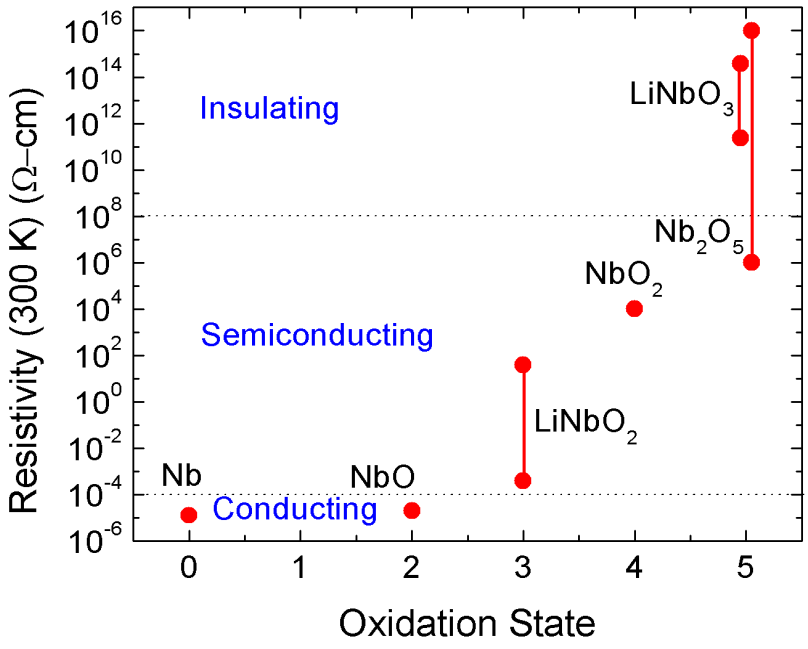

Figure 1 Various niobium oxides and lithium niobium oxides as a function of resistivity. As the niobium oxidation state increases the material becomes more insulating, with the various materials spanning the resistivity range.

Molecular Beam Epitaxy (MBE) provides monolayer control and high quality material. However, the growth of stoichiometric refractory metal oxides by MBE is traditionally difficult because of inadequate oxygen and low vapor pressure metal sources leading to extremely low growth rates [26]. Transition metals are difficult to evaporate controllably due to high temperature requirements and the poor compatibility of a hot electron beam filament with an oxygen environment. $LiNbO_3$ is very difficult to grow stoichiometric in oxygen, and it is often annealed post-growth to incorporate more oxygen in the film [27]. It is difficult for any niobium film to reach full oxidation in an MBE environment at the high growth temperatures required for quality single crystalline material, and therefore a more reactive oxidizer is desirable to reach these fully oxidized states. Previous work has explored oxidizers such as oxygen plasmas and dangerous ozone sources to achieve highly reactive species O and O_3 [28]. This work investigates lithium perchlorate, $LiClO_4$, as a solid/liquid state oxygen source alternative to these gas based methods, as well as a new style of MBE effusion cell for the evaporation of metal-halide sources which offer much lower evaporation temperatures and therefore greater flux stability [29].

1.2 Molecular Beam Epitaxy

Molecular Beam Epitaxy, pioneered in the late 1960's and early 1970's, is a method for thin film epitaxy similar to evaporation where thermal molecular beams are directed at a crystalline substrate under high to ultra-high vacuum (UHV) conditions [30-33]. Knudsen effusion cells are used to control source material temperature, and therefore flux rates, according to the material specific vapor pressure-temperature curves. The sources are individually shuttered, providing single monolayer control of layer

thicknesses and allowing the growth of abrupt heterointerfaces and superlattices. In the UHV environment, atomic or molecular vapor travel in a beam directed at the substrate with virtually no collisions due to a large mean free path on the order of 10^5 m under UHV at 10^{-9} torr. When gases are injected into the system as a growth constituent growth pressures can rise to 10^{-5} torr, however the mean free path is still on the order of 1 m indicating that all collisions and reactions are occurring at the substrate surface. The crystalline substrate is heated in typical applications to increase the surface diffusion of adatoms which ideally migrate to step edges, templating the growing thin film epitaxially onto the substrate. Liquid nitrogen cryo-shrouds are often used in these systems to locally adsorb gases around the growing film to minimize impurities.

MBE benefits from several *in situ* characterization techniques which allow real time feedback of the growth conditions and of the structural nature of the growing film. Among these techniques the most widely used is Reflection High Energy Electron Diffraction (RHEED), a technique where high energy electrons are directed at the growing film at an oblique angle and the diffraction pattern is monitored on a phosphor screen opposite the electron source. In this technique the electrons are diffracted by crystalline planes onto the screen in a pattern related the lattice reciprocal space. A smooth surface is indicated by intense streaks, while a rough surface scatters the electrons and appears as a series of spots. The intensity of these streaks and spots oscillates for every monolayer grown, allowing precise control over the number of monolayers deposited [32]. A well calibrated system can also be used to extract lattice constants by measuring streak separation in reciprocal space.

MBE was originally used for the growth of GaAs, AlAs, and AlGaAs ternary tunable alloys [31, 32, 34], but has since been applied to various other material systems such as the HgCdTe tunable ternary [35], the nitride family, GaN, InN, AlN, and their ternaries[36], and functional oxides [37]. This work is concerned with the growth of functional oxides by MBE.

1.3 Lithium Assisted Growth by Metal-Halides: Niobium (V) Chloride

Historically, refractory metals have been evaporated by electron beam to achieve growth level fluxes in MBE; however, the hot filament used to create the electron beam oxidizes and breaks easily in an oxide growth environment. For this reason, niobium oxides have been previously deposited using a lithium assisted metal-halide growth chemistry [11, 27, 29]. In this method the niobium source is $NbCl_5$, present as the dimer Nb_2Cl_{10}, which has an equilibrium vapor pressure of ~1×10^{-4} torr at 20 °C. The chlorine from $NbCl_5$ is gettered by lithium forming LiCl that desorbs from the substrate surface at growth level temperatures (vapor pressure = 3.61 torr at 900 °C). This growth method is described in depth by *Doolittle et. al* [27], *Greenlee et. al* [11] and *Henderson et. al* [29]. In this previous work, the material was evaporated from a Createc NATC-40-40-290 oil/water heated cell, which provided temperature stability of ~0.1%. Despite this stability, radiation from the hot substrate (~900 °C) caused the $NbCl_5$ cell temperature to rise, increasing the growth rate gradually over the course of the growth.

To overcome this issue, a new type of evaporation cell is necessary. The requirements of this cell will be a temperature stability of 0.1 °C over the required temperature range (25-75°C) and thermal isolation from the hot substrate so that upon

shutter opening the bulk of the cell will not drift in temperature causing an unwanted increase in vapor flux.

1.4 Lithium Perchlorate

Previous work has indicated that oxygen incorporation into a niobium oxide films at high temperatures (> 650 °C) is difficult, with the fully oxidized state of niobium (chemical valence +5) difficult to achieve. $LiNbO_3$ films have been grown by MBE in the past, as well as the ceramics Li_3NbO_4 and $LiNb_3O_8$, but the repeatability of these growths is poor due in part to low and variable oxygen incorporation [27]. This oxygen incorporation issue has led to the exploration of a stronger oxidizer than molecular oxygen, lithium perchlorate ($LiClO_4$), as an alternative to a higher reactivity sources such as ozone and oxygen plasmas which require a very specific flow control and in the case of the former extensive safety regulation due to reactivity. Lithium perchlorate has the highest volumetric density of oxygen of any material, including liquid oxygen. The volumetric density of oxygen for several chemical oxygen generators is shown in Table 1. Lithium perchlorate is also the only member of the perchlorate family that is stable above its melting point [38], meaning that it will form a liquid before decomposing while all others sublime.

Table 1. Density, mass percentage, and oxygen volumetric density of various materials used to evolve oxygen gas including lithium perchlorate and liquid oxygen, sorted by oxygen volumetric density. Adapted from Peters et al. [38]

Material	Density (g/cm^3)	Mass % O_2	Grams O_2 gas per cm^3
$LiClO_4$	2.43	60.1	1.45
$NaClO_4$	2.53	52	1.31
$KClO_4$	2.52	46.2	1.16
$LiClO_3$	1.12	53	0.59
$NaClO_3$	2.49	45.1	1.13
$KClO_3$	2.32	39.2	0.91
98% H_2O_2	1.43	46.1	0.66
Liquid Oxygen	1.14	1.14	1.14

Lithium perchlorate is traditionally used as a chemical oxygen generator for emergency oxygen candles as well as a method of chemical oxygen storage [38, 39]. In this form, lithium perchlorate exists in the solid form with a binder and a small mole fraction of fuel such as magnesium which provides the heat for the decomposition of oxygen. Lithium perchlorate is also highly soluble in a number of solvents and is used in this form as a soluble electrolyte for lithium ion batteries.

Lithium perchlorate exists in the solid state as salt granules at room temperature. The substance melts at 236 °C in its anhydrous form, although it is highly hygroscopic and should be handled in a dry environment. Once hydrated (lithium perchlorate forms both a mono- and trihydrate) the anhydrate can be reclaimed by heating the system to above 145.75°C [40]. Lithium perchlorate begins to decompose near 400 °C, with the

reaction becoming exothermic around 420 °C [38, 41, 42]. The material decomposes according to equations (1)-(3).

$$LiClO_4(l) \rightarrow LiCl(sol.) + 2O_2(g) \quad (1)$$

$$LiClO_4\,(sol.) + LiCl(sol.) \rightarrow LiClO_3\,(sol.) + LiCl(sol.) + O(g) \quad (2)$$

$$LiClO_3(sol.) \rightarrow LiCl(sol.\text{ or }s) + {}^3/_2\,O_2(g) \quad (3)$$

The decomposition of $LiClO_4$ is autocatalytic, catalyzed by the product LiCl [41], where the formation of LiCl is thought to assist in rupturing the Cl-O bond. This rupture theory is consistent with an observed activation energy of 222 kJ [42]. The decomposition is shown to simplify to a standard first order reaction at a LiCl composition of ~40%, at which point the solution is saturated. Equations (2) and (3) indicate both molecular and atomic oxygen species are evolved during the decomposition process. The presence of atomic oxygen provides the potential for higher reactivity and stronger oxidation. The LiCl autocatalysis necessitates preconditioning the material by prolonged heating or pre-mixing of LiCl to reach the 40% LiCl saturation point. In addition, the 400 °C decomposition temperature places an upper limit on the operational temperature of the cell as well as the temperature ramp rate to prevent local heating exceeding the full decomposition temperature.

DESIGN AND CHARACTERIZATION

2.1 Niobium (V) Chloride

2.1.1 Cell Design

A new effusion cell has been designed for the evaporation of high vapor pressure $NbCl_5$ and manufactured by VESCO-NM. The cell, shown in Figure 2, has a bulk material zone that is, like the former cell, temperature controlled by an oil or water bath to maintain stable temperatures in the near-ambient range [29]. A second heating zone was added at the tip of the cell, controlled by a traditional filament, which along with an aperture plate provide thermal isolation from the substrate radiation. The hot zone also prevents condensation on the aperture plate and allows a back pressure of $NbCl_5$ for more stable flux control. Both zones have separate thermocouples for individual control, and the liquid bath responsible for heating and cooling the bulk is temperature controlled by a sensor on the output port of the cell. The crucible is an elongated quartz tube, which is filled half full of material to avoid evaporation from the hot zone. The aperture plate consists of a 5x5 hole pattern to restrict flow and provide more uniform flux, and is made of PBN.

Figure 2 a) Custom NbCl5 cell with **b)** tip filament, bulk water, tip and bulk thermocouple feedthroughs, and **c)** a 5x5 hole pattern aperture plate.

The $NbCl_5$ cell has been attached to a 2 ¾" con-flat source flange on a Varian Gen-II MBE system. The material is loaded in a dry nitrogen atmosphere to prevent formation of corrosive HCl and Nb_2O_5 due to exposure to moisture in the air according to the reaction shown by Equation 4 which is calculated as energetically favorable at room temperature with a change in Gibbs free energy of -45.89 kcal at 0 °C.

$$2NbCl_5 + 5H_2O\ (g) \rightarrow 2Nb_2O_5 + 10HCl\ (g) \quad (4)$$

2.1.2 Cell Characterization

The vapor flux from the new cell design, measured in beam equivalent pressure (BEP), follows a linear trend with temperature on an Arrhenius plot, shown in Figure 3, as is expected for Knudson flow. Growth level $NbCl_5$ fluxes can be achieved at 30-60 °C compared to previous work at 25-35 °C, indicating flow retardation by the aperture plate. After 6 months of use, the aperture plate shows no corrosion or clogging, indicating the hot zone operating temperature of 100-150 °C is sufficient to prevent any condensation. The cell was measured for long term flux stability over a period of 24 days, shown in Figure 4, and shows stability within the quoted error range of a standard ion flux gauge (20% within a pressure decade), indicating that flux drift is reasonably controlled with this design.

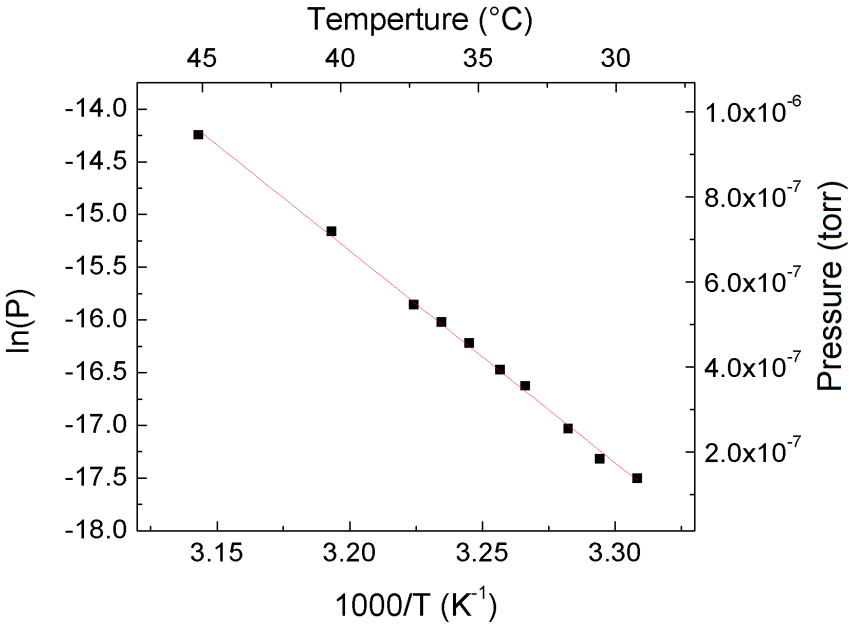

Figure 3 The measured $NbCl_5$ flux (BEP) versus temperature on an Arrhenius plot follows an expected linear trend. Growth level fluxes occur above ~30 °C. The included fit gives an equation $\ln(P) = 49.0 - 20.1 \frac{1000}{T(K)}$

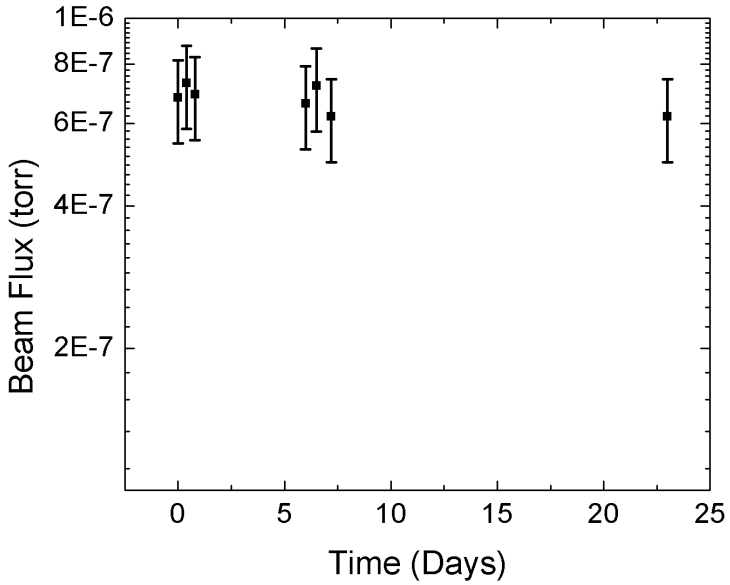

Figure 4 Measured $NbCl_5$ flux at a single setpoint over a period of 24 days. The cell remains stable within the error range (20%) of a standard ion flux gauge, depicted by error bars ($\sigma = 4.39 \times 10^{-8}$ torr).

2.2 Lithium Perchlorate

2.2.1 Design Constraints

The $LiClO_4$ material has been loaded into its own standard Knudsen effusion cell. The material has been loaded into a modified custom crucible shown in Figure 5 made of beryllia (BeO), due to previous research which indicated that a niobium crucible would corrode and that PBN would swell by lithium intercalation.

Figure 5. Custom beryllia crucible made to hold LiClO4 in a Knudsen effusion cell. Previous work has indicated that $LiClO_4$ will corrode anything that can oxidize, and Li will intercalate into and swell PBN.

2.2.2 Material Characterization

Oxygen evolution begins shortly after the material melts, with growth level fluxes of oxygen obtained at cell temperatures between 250 and 350 °C. The measured flux is shown on an Arrhenius plot in Figure 6 for the range 250 to 325 °C, showing the expected linear trend with a measured flux of approximately 1.5×10^{-5} torr at 325 °C.

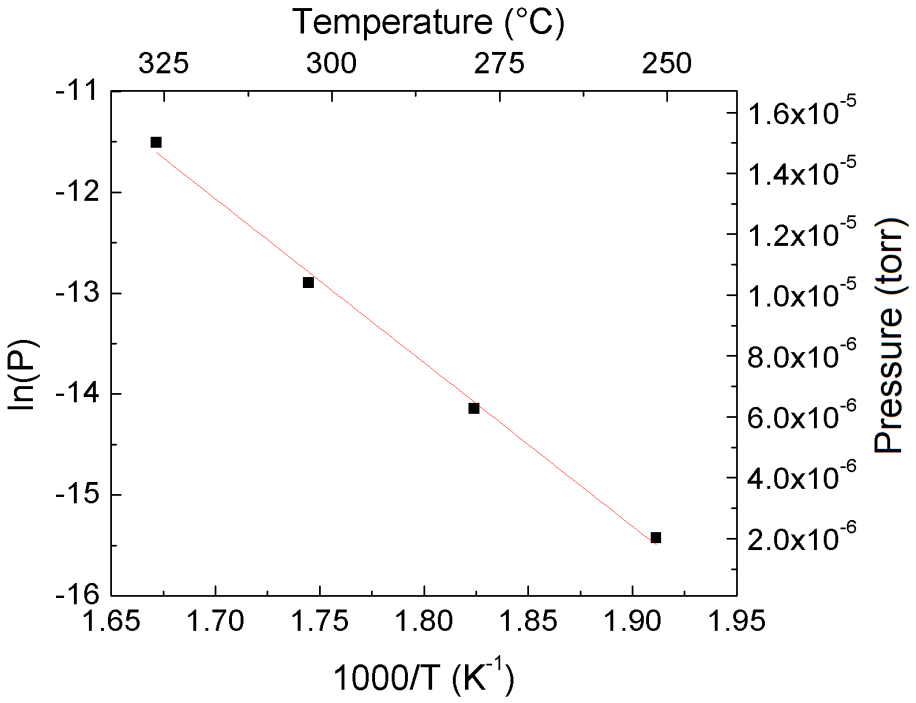

Figure 6 The measured $LiClO_4$ flux (BEP) versus temperature on an Arrhenius plot follows an expected linear trend. Growth level fluxes occur above ~250 °C, the approximate temperature at which oxygen evolution begins. The included fit gives an equation $\ln(P) = 15.5 - 16.2 \frac{1000}{T(K)}$

In situ Auger Oxidation Rate Studies

To quantify the oxidation rate of niobium using the $LiClO_4$ oxygen source, the oxygen KLL Auger peak is monitored for changes in overall intensity. An *in situ* Auger probe (Staib Instruments) is used to examine reactions on the surface of the growing film by Auger Electron Spectroscopy (AES). In this configuration, an electron probe is used to analyze Auger electrons excited by the RHEED gun and the probe is mounted in the pyrometer port of a Varian Gen II MBE system normal to the substrate. AES is a surface sensitive technique, and the *in situ* Auger Probe uses glancing angle electrons from the RHEED gun making the technique highly surface sensitive and therefore sensitive to the oxidation reaction at the surface of the thin film [43]. This particular system has shown sub-monolayer surface sensitivity to changing elemental compositions [4, 43]. Unlike traditional Auger systems, the Staib Auger probe supplies the direct, non-differentiated signal representing the E×N(E) spectra. In this experiment, crystalline BCC Nb is deposited on sapphire, growth is halted, and the surface is exposed to oxygen while monitoring the Auger signal in real time. Upon opening the $LiClO_4$ shutter, the oxygen KLL peak immediately begins to intensify. When plotted against time the Auger peak height follows a first order exponential relation, saturating as the surface reaction comes to completion as shown in Figure 8. The Auger peak height is proportional to the overall number of oxygen KLL auger electrons which is directly related to the number of oxygen atoms present in the energized volume, which increases exponentially toward a saturated value representing the final (but not necessarily full) oxidation state. In a similar work Sanz et. al [44] exposed niobium and tantalum films to controlled oxygen fluxes *at room temperature* and monitored the oxygen KLL auger signal to determine reaction trends,

coming to the conclusion that at room temperature oxidation proceeds in multiple regimes, forming both suboxides and fully oxidized films. The findings of this work are summarized in Table 2.

Table 2 Summary of Sanz et. al [44] study of the oxidation of niobium at room temperature.

Oxygen dose (Langmuir)	Result
0-2 L	Rapid uptake of oxygen below the metal surface
2-7 L	Formation of 2 – 3 monolayers of the suboxides NbO and NbO_2 on the surface of the film.
>7 L	Formation of Nb_2O_5 covering the suboxide layer.

Multiple data points are taken from 40 eV wide scans of the oxygen KLL peak with a resolution of 0.5 meV. The measurement time is 30 seconds. Scatter plots are fit to a first order exponential following the form of Equation 5, where measured peak intensity is taken from the E×N(E) spectra, shown in Figure 7.

$$I = I_0 - Ae^{-\frac{t}{\tau}} \tag{5}$$

I_0 is the final peak height, t is time, τ is the time constant characteristic of the oxidation, and A is a fitting constant not equal to I_0, indicating a non-zero initial concentration of surface oxide due to background level oxygen in the MBE system.

Characteristic oxidation peak height transients are shown in Figure 8 for 0.5 SCCM diffuse O_2 and $LiClO_4$ at 300 °C. While these two transients have similar time

constants, the measured beam flux for $LiClO_4$ is about 4 times lower than that of diffuse O_2. It is theorized that the mixture of molecular and atomic species present in the $LiClO_4$ oxygen evolution allows faster oxidation, providing the possibility of faster growth rates for oxide films than previously possible.

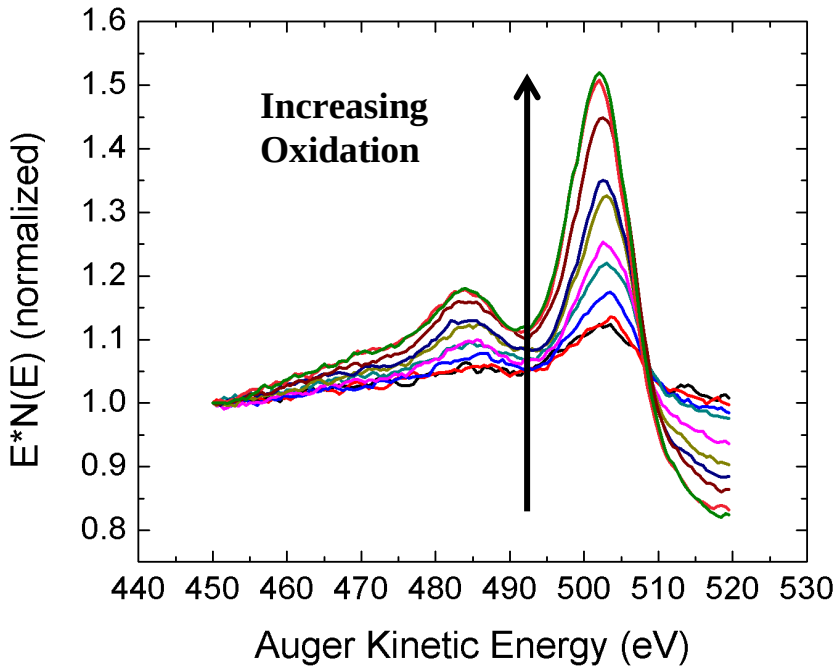

Figure 7 Successive Auger oxygen KLL peak height scans showing increasing surface oxidation.

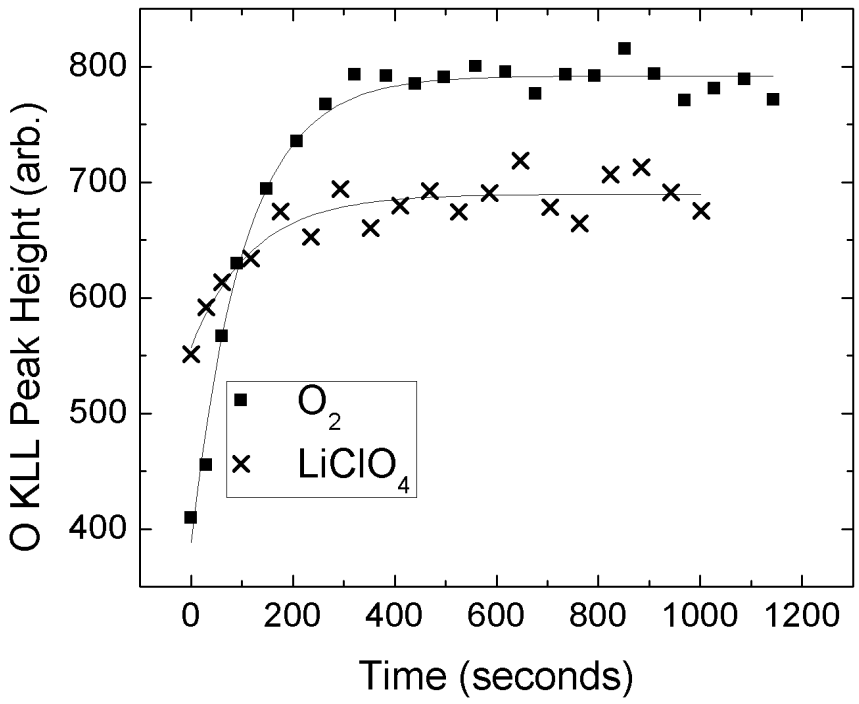

Figure 8 Auger oxygen KLL peak height as a function of time. The included fit is a first order exponential, characteristic of the oxidation time constant for the given system for a) $LiClO_4$ at 300 °C, beam flux 8 × 10-7 torr, τ = 120s, and b) 0.5 SCCM diffuse O_2, beam flux 3×10^{-6} torr, τ = 110 s.

Pressure Instabilities

During the operation of the $LiClO_4$ cell, pressure variations become an issue significantly affecting the overall chamber pressure. Once oxygen evolution begins at approximately 250°C the pressure in the growth chamber, as measured by cold cathode gauge, rises sharply with the decomposition of the $LiClO_4$ bulk material. The oxygen RGA signal also becomes noisy, varying around its mean by ~ $\pm 5 \times 10^{-8}$ torr. Monitoring residual gas analysis (RGA) signals at mass to charge ratio 32 for oxygen and 16 for doubly ionized oxygen and molecular oxygen, as shown in Figure 9, the same noise is observed indicating that oxygen is the source of the pressure variations. These pressure variations are not present for gas source molecular oxygen indicating that the RGA signal

from $LiClO_4$ is relevant. Other monitored signals such as water, carbon dioxide, and hydrogen do not show these noise trends.

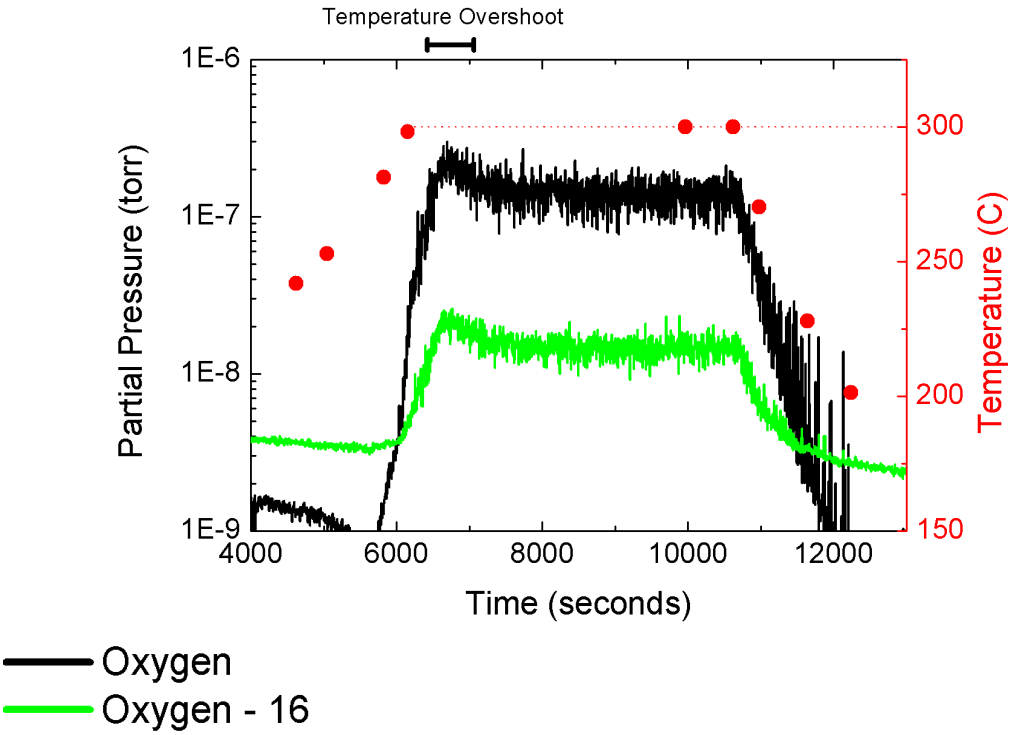

Figure 9 RGA partial pressures measured at mass to charge ratio (m/q) 32 (black) and 16 (green) as the $LiClO_4$ cell is heated to 300°C (temperature shown in red), held constant for 1 hour, and then subsequently cooled.

While the source of the pressure instabilities is unknown, some hypotheses can be made about the origin and solutions to the problem. Pressure instabilities could be caused by bubbling from the crucible sidewall as the oxygen evolution occurs, causing droplets of liquid $LiClO_4$ to spit from the cell. If true, then a valved or aperture sealed cell such as the $NbCl_5$ cell described in this work could resolve these instabilities, allowing a back pressure of oxygen to develop for more uniform flow. Previous reports of chemical additives used to stabilize the decomposition of $LiClO_4$ such as $AgNO_3$ and $AgClO_4$ could also be used to reduce the pressure fluctuations [45].

Comparison with Molecular Oxygen

RGA signals exhibit specific cracking patterns for various materials relating to the probability of double ionization as well as the probability of cracking a dimer such as O_2. For molecular oxygen, the measured ratio of the RGA signals at mass to charge ratio 16 to 32 is 5.67%, while that ratio is 8.42% for $LiClO_4$. This corresponds to a 48.5% increase in signal at mass to charge ratio 16. This increase supports the mixed oxygen species theory, suggesting that the $LiClO_4$ is evolving both molecular and atomic oxygen. It is hypothesized that this is the mechanism behind the faster oxidation rate per flux beam equivalent pressure revealed by the *in situ* Auger transient experiment.

FILM GROWTH

3.1 Characterization by X-Ray Diffraction

For all films grown, X-Ray Diffraction (XRD) is the primary method of crystalline phase identification due to the superior amount of information which can be obtained, ease of use, and the exhaustive existing database of characterized materials. While most phases are easily identified in XRD based on a cursory knowledge of the material being scanned, niobium oxides provide a challenge due to the existence of many suboxide and oxide phases of similar crystal structure. $LiNbO_2$ (002), Nb_{BCC} (110), and $LiNbO_3$ (006) are all easily identified, while the other possible phases are not. Table 3 lists the various possible phases and their XRD peak locations based on Cu-K_α radiation (λ = 1.54056 Å). There are five possible phases in the narrow range 36.772 – 37.069 degrees 2θ-ω, and 3 of those materials fall within 0.4 degrees of each other, making phase identification extremely difficult. It is possible to differentiate them all, however, using multiple XRD scans as well as knowledge of the material in question. FCC oriented niobium films can generally be ruled out of oxide film growth due to the tendency of niobium to react with oxygen, reducing the number of possibly degenerate oxide phases to four. Niobates with valence +5 are typically transparent ceramics, and in certain situations can be visually distinguished from suboxide states. $LiNb_3O_4$ and Li_3NbO_8 both have valence Nb^{+5} and are often identified by transparency, while NbO and NbO_2 will not be transparent. The Li_3NbO_8 reflection within the 2θ-ω range in question is the (600) reflection and has a corresponding (400) and (800) allowed reflection which can help to distinguish it from $LiNb_3O_8$ assuming the intensity of the peaks are large enough. If visual transparency confirmation is not possible, the phases may be distinguished by asymmetric off-axis

scans using XRD. While NbO and $LiNb_3O_4$ are both cubic and separated in 2θ-ω by only 0.036 degrees, the NbO reflection is (111) while the $LiNb_3O_4$ reflection is (222), resulting in a doubling of the Li_3NbO_4 peaks in reciprocal space. NbO_2, having a different crystal structure and oriented to the a-plane, is easy to identify by this method.

While the previous method describes a procedure for discerning each individual phase from another, it is not always easy to put in to practice. The values listed in Table 3 are ideal bulk values, while many films grown are under considerable epitaxial strain causing these values to shift. Niobium oxides often exist in oxygen poor phases which can also shift the d-spacing of the material, and in phases where lithium is not chemically bound it can act as a defect, shifting the lattice spacing. Due to these difficulties the materials to be analyzed in the following section are not always exhaustively identified but rather referred to as an "unwanted suboxide". Any phase that is definitively identified is labeled by its chemical name.

Table 3. X-Ray Diffraction reflections, structure, and chemical valence for various niobium and niobium oxide films. λ=1.54056 Å for Cu-K_α radiation.

Material	Structure	Nb Valence	2θ-ω	h k l
$LiNbO_2$	Hexagonal	+3	16.941	0 0 2
$LiAlO_2$	Rhombohedral	+5	18.68	0 0 3
$LiNb_3O_8$	Orthorhombic	+5	24.42	4 0 0
LiNbO2	Hexagonal	+3	34.267	0 0 4
Nb_2O_5	Monoclinic	+5	35.998	0 0 7
Nb	FCC		36.772	1 1 1
NbO	Cubic	+2	36.953	1 1 1
Li_3NbO_4	Cubic	+5	36.989	2 2 2
$LiNb_3O_8$	Orthorhombic	+5	36.993	6 0 0
NbO_2	Tetragonal	+4	37.069	4 0 0
Nb	BCC		38.475	1 1 0
$LiNbO_3$	Rhombohedral	+5	38.949	0 0 6

3.2 Niobium Thin Films

Niobium is a type-II superconductor and one of a few elemental superconductors such as tin, lead, vanadium, and technetium, where most superconductors are alloys. It undergoes the superconducting transition at T_c = 9.25 K [46]. Niobium and niobium alloys are of particular importance because they are the primary materials used in Josephson tunnel junctions [47]. Niobium thin films have previously been grown on sapphire substrates by MBE using electron beam heated sources [48].

Niobium films have been grown, using the new near ambient two-zone cell described in section 2.1, on sapphire substrates by lithium assisted growth chemistry. The $NbCl_5$ cell is operated at a tip temperature of 130 °C, while the bulk is maintained at 50 °C by a heated recirculating water bath, with a measured flux by ion gauge of ~ 7×10^{-7} torr. The $NbCl_5$ is reduced to Nb with a coincident Li flux, which is maintained in the

range of 5×10^{-7} torr and varied to adjust the growth rate. Films are deposited slowly, at approximately 20 - 50 nm/hr at a substrate temperature of 850 – 950 °C. The Nb thin films are analyzed for crystalline quality using a Panalytical MRD XRD system (Cu-K_α). The Nb nucleates (110) oriented BCC on c-plane sapphire, indicated by the diffraction scan shown in the inset of Figure 10. The presence of Pendellösung fringes indicates a smooth film. The film also exhibits an omega rocking curve FWHM of ~130 arcseconds, shown in Figure 10, indicating excellent crystal quality. Secondary Ion Mass Spectroscopy (SIMS) profiling of the films show no chlorine or lithium contamination with the signals for both elements below the detection limit of the spectrometer.

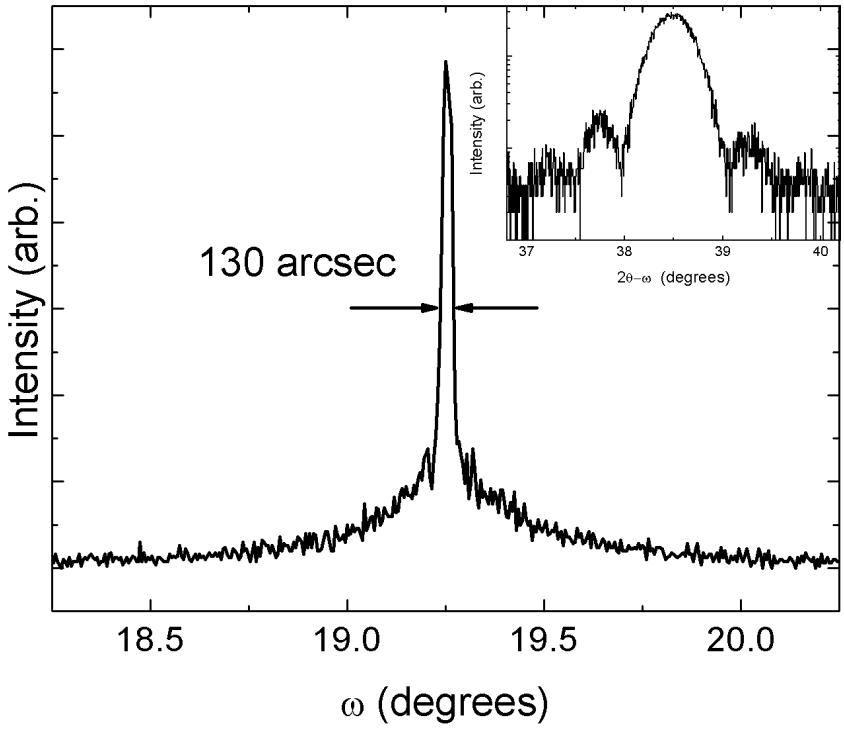

Figure 10 XRD rocking curve of the BCC Nb film with a FWHM of 130 arcseconds indicating excellent crystalline uniformity. **Inset** X-ray Diffraction scan showing (110) oriented BCC Nb with Pendellösung fringes indicating a smooth film.

3.3 Niobium (II) Oxide

Nb oxidized in the +2 valence state forms NbO, which is normally an unstable compound. NbO typically exists as an intermediate oxide layer in the formation of Nb_2O_5 on Nb in the presence of oxygen [44, 47]. NbO is a semi-metal with a resistivity on the order of 10^{-5} Ω-cm as noted in Figure 1 [49], and is cubic in the *Pm3m* space group with a lattice parameter a = 4.21 Å. The unit cell is a derivative of rocksalt structure, with the exception of having 25% ordered vacancies of both cations and anions [49, 50].

NbO has been grown by limiting the Li cell to fluxes where all of the lithium is consumed by cracking $NbCl_5$ and forming desorbing LiCl rather than incorporating in the film. Lower oxygen pressures are used to promote the metastable phase and films are grown around 850 °C. Figure 11 shows a characteristic NbO film grown by this method. The film in Figure 11 is approximately 100 nm thick and is grown slowly to encourage growth of the suboxide, and shows a γ-$LiAlO_2$ (003) oriented interface layer related to Li reaction with the Al_2O_3 substrate. The omega rocking curve of the NbO film is ~1200 arcseconds, a large value indicating crystalline degradation, most likely due to a large mismatch with the substrate which has a hexagonal a-spacing of 4.785 Å compared to the film's 2.977 Å pseudo-hexagonal lattice constant, leading to a mismatch of nearly 25%.

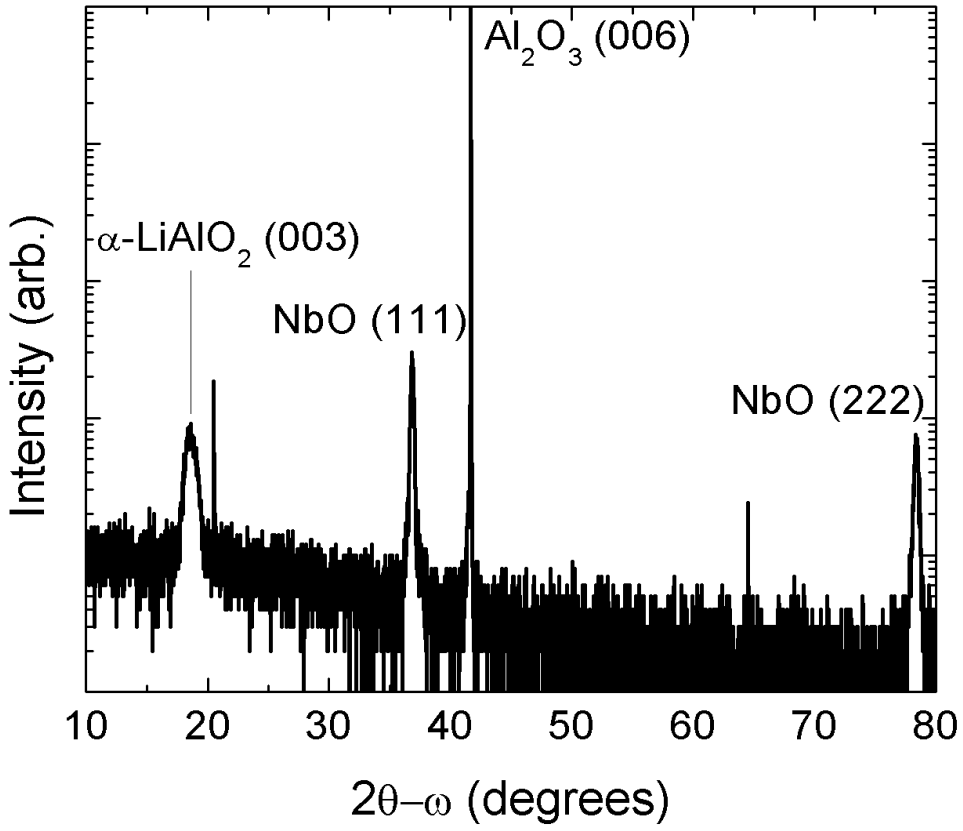

Figure 11. XRD 2θ-ω scan of (111) oriented NbO with an interface layer of α-$LiAlO_2$.

3.4 Lithium Niobite

The material of most importance is the Li intercalated suboxide $LiNbO_2$, which is interesting for its potential use as a biologically realistic synapse for neuromorphic computing architectures among other interesting properties and applications [10-16, 18-23]. McDowell et. al. state that $LiNbO_2$ may have undetermined unusual electronic properties due to the lack of suitable explanations for its strange behavior including difficulty rationalizing the electrical resistivity of the material [51]. These unanswered questions, along with the possibility of remarkable properties and applications, make $LiNbO_2$ an exciting research candidate for next-generation materials and systems.

The basic experimental plan for the growth of $LiNbO_2$ is based on the methods outlined by Henderson et. al. [29], namely the use of constant oxygen and niobium flux while varying lithium flux to adjust oxygen incorporation into the film and therefore final oxidation state. Oxygen partial pressures of approximately 10^{-7} torr were targeted for films grown with $LiClO_4$ as the oxygen source. A $NbCl_5$ flux of approximately 10^{-6} torr was targeted for all depositions, corresponding to approximately 50°C in the bulk zone of the two zone effusion cell. The effects of lithium flux and substrate temperature were studied.

3.4.1 Substrate Temperature Dependence

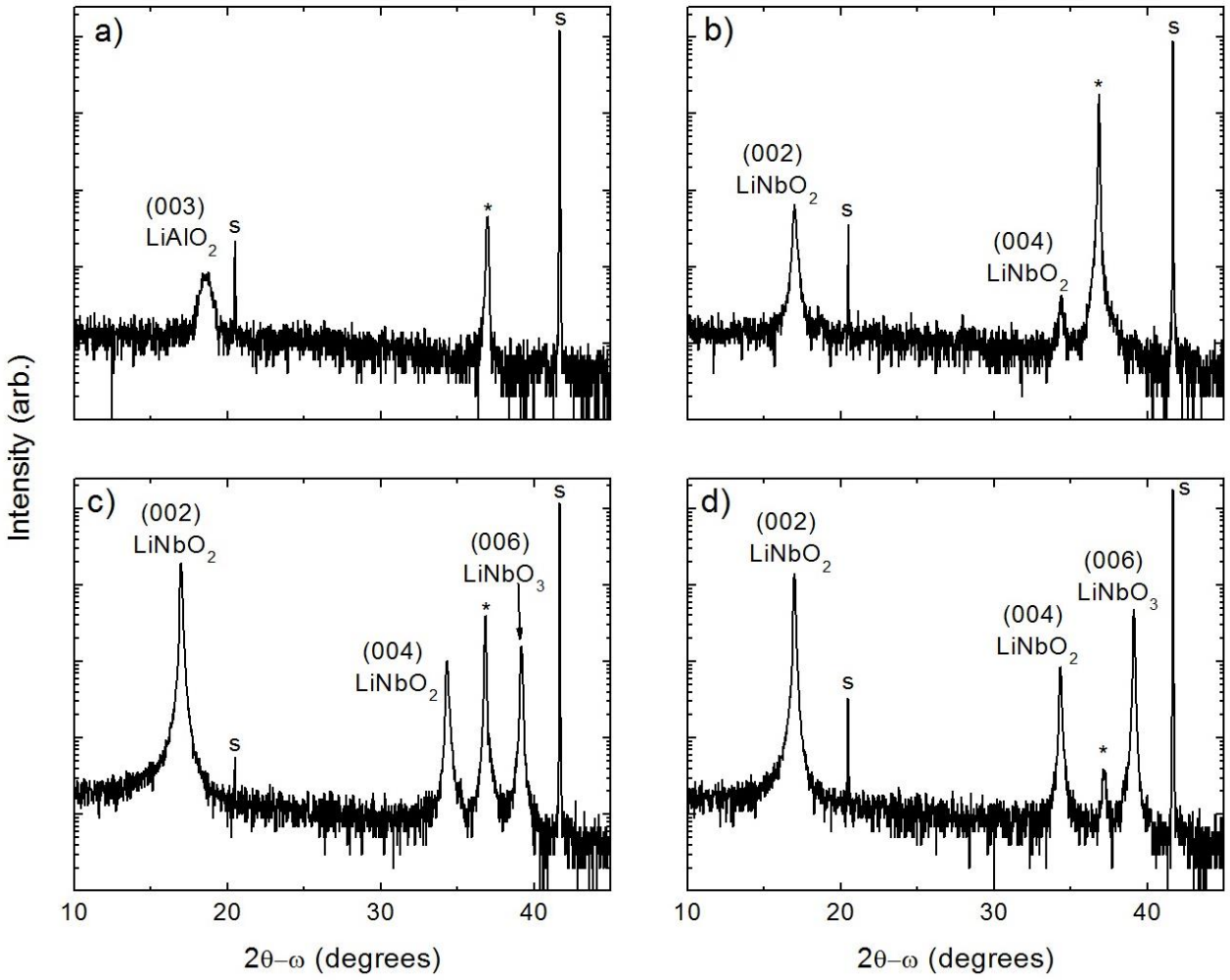

Figure 12. X-ray diffractograms of films grown on c-plane sapphire (denoted "s") at different substrate temperatures (a) 850 °C, (b) 900 °C, (c) 950 °C, and (d) 1000 °C showing increasing $LiNbO_2$ crystallinity and decreasing crystallinity of various other phases with increasing temperature. (*) various possible unwanted niobium oxide phases falling within the range $36.8 < 2\theta\text{-}\omega < 37.2$ degrees.

Previous results showed $LiNbO_2$ could be grown at a substrate temperature of 850 - 900°C [11, 29], and experiments were initially conducted around this temperature range. Figure 12 shows X-ray diffractograms of films grown from 850 – 1000°C in 50°

increments. For the 850 °C sample no $LiNbO_2$ is found, only γ-$LiAlO_2$ and an unwanted niobium oxide phase. Increasing the substrate temperature to 900 °C results in $LiNbO_2$ growth with an (002) omega rocking curve of 493 arcseconds, however an unwanted niobium oxide phase is present in majority by overall XRD counts with a 152 arcsecond omega rocking curve. Further increasing the substrate temperature to 950 °C provides a dramatic improvement in the $LiNbO_2$ XRD signature where the (002) peak is present in majority with a 337 arcsecond omega rocking curve along with unwanted niobium oxide phases. At this substrate temperature $LiNbO_3$ growth also occurs with a 209 arcsecond omega rocking curve. Finally, taking the substrate to 1000 °C, as shown in Figure 12 (d), produces similar quality $LiNbO_2$ with an omega rocking curve of 318 arcseconds as well as a diminished unwanted suboxide phase. The $LiNbO_3$ phase however is larger than the previous cases, and shows a 240 arcsecond omega rocking curve. Despite a larger $LiNbO_3$ signature by XRD, the sample in Figure 12 (d) grown at 1000 °C represents the best case, and further experiments will optimize around this point.

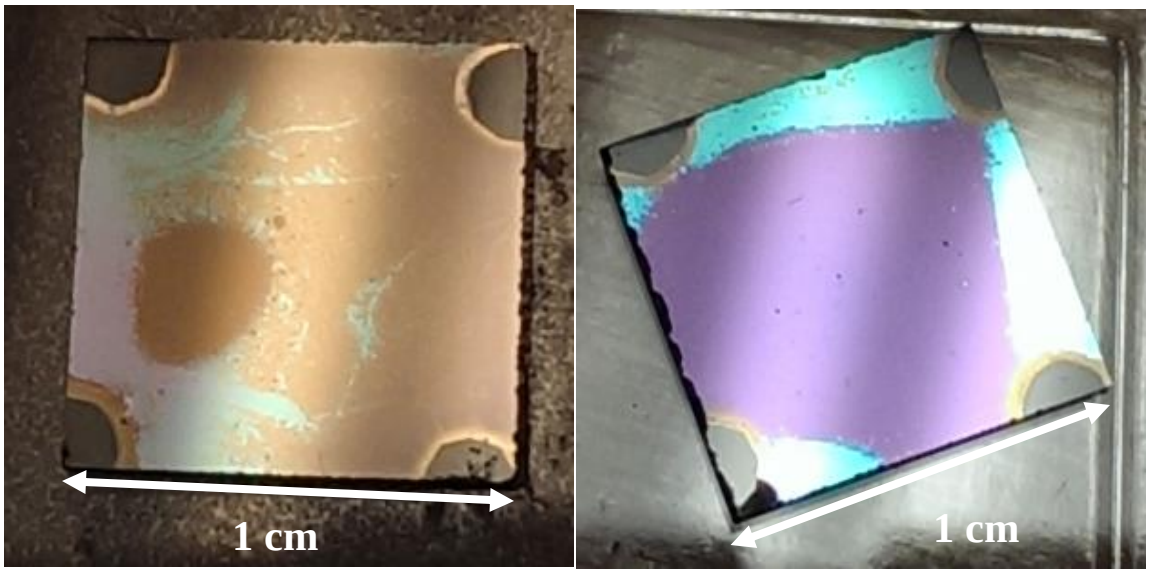

Figure 13. $LiNbO_2$ films grown at (a) 950 °C and (b) 1000 °C showing multiple phases physically separated across the surface of the wafer. The square in the center of (b) aligns with the square hole in the mounting plate.

It is important at this point to note the appearance of the previously mentioned films. Figure 13 (a) shows the 950 °C film represented in Figure 12 (c). Significant non-uniformity in color is apparent across the surface of the film, indicating physical separation of phases and a gradient of some kind across the substrate rather than competing intermixed phases. The feature becomes more apparent for the 1000 °C film, shown in Figure 12 (d) and Figure 13 (b). The diffractogram shows an intense $LiNbO_2$ peak, a significantly diminished unwanted suboxide peak, and a large $LiNbO_3$ peak. This primarily two-phase composition is confirmed by Figure 13 (b), showing a large central dull purple square with bright reflective blue edges. Under transmitted light the blue edges appear red and the center appears dull grey, the former of which could correspond to $LiNbO_2$ with a reported bandgap in the red range of 1.4-2.04 eV [21, 29, 52-57]. The square shape visible on the film surface corresponds to the square hole in the back of the

mounting plate, indicating that a temperature gradient is possibly responsible for the physical separation of the phases. It is therefore hypothesized that single phase material will not be possible to obtain without modifying the substrate heater or mounting apparatus to provide more uniform heating, or a larger wafer to allow growth in the more uniform area of the heater. To address this problem several solutions have been proposed: (1) Using a solid back mounting plate as a heat diffuser, (2) using a sapphire back mounting plate as a heat diffuser, (3) installing a different substrate heater, and (4) growing on larger wafers and removing unwanted portions by dicing or scribing. Solution 1 was quickly ruled out due to poor film quality. All films grown with the solid back mounting plate were $LiNb_3O_4$ with high rocking curves (~ 1 degree), lithium poor films with poor crystallinity, indicating that re-radiation from the back mounting plate and the absorbing backside metallization on the wafer were responsible for too much radiative heat loss. Solution 3 requires system maintenance involving a long bake cycle, and solution 4 involves the custom fabrication of new mounting plates. Therefore solution 2 was chosen as the next option for growth improvement. Sapphire is transparent at room temperature, but the absorption coefficient increases for increasing temperature. For the blackbody spectrum maximum at 1273 K of ~2.3 μm the absorption coefficient is over 3 times larger than the coefficient at room temperature [58]. While the material is still translucent, the added thickness and increased absorption coefficient allow sapphire to act as a heat diffuser plate. Due to displacement of the thermocouple from the sample by the new back mounting plate, substrate temperature was controlled by power to reach the same approximate temperatures. It should be noted that irregularities

in back plate size and mounting blocks could cause different substrate temperatures when controlling by power.

3.4.2 Lithium Flux Dependence

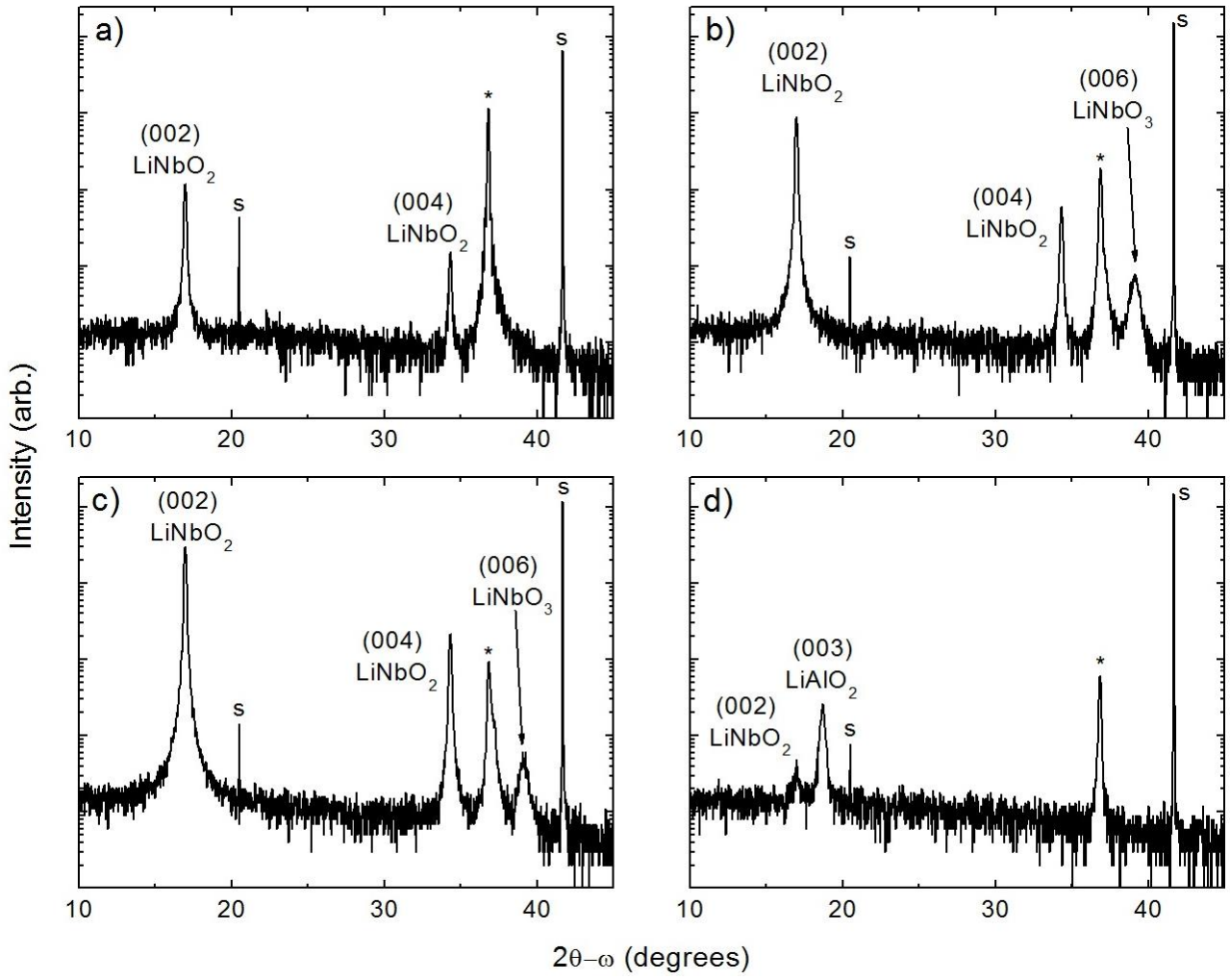

Figure 14. X-ray diffractograms of films grown on c-plane sapphire (denoted "s") at different Li cell currents (a) 6A, (b) 6.25A, (c) 6.5A, and (d) 7A showing increasing $LiNbO_2$ crystallinity and decreasing crystallinity of various other phases with increasing Li flux up to 6.5A and almost no discernable $LiNbO_2$ at 7A. (*) various possible unwanted niobium oxide phases falling within the range $36.8 < 2\theta\text{-}\omega < 37.2$ degrees.

With a new substrate power condition and sapphire back mounting plate, the previous 1000 °C experiment was repeated, the results of which are shown by X-ray diffractogram in Figure 14 (a). The $LiNbO_2$ omega rocking curve was approximately the same, at 375 arcseconds, but the largest peak is now the unwanted niobium suboxide, and the $LiNbO_3$ phase is not resolved. It is possible that a shift in condition, most likely thermal, has changed the growth rate of the material or sticking coefficient of one or multiple flux constituents, or possibly the nucleation conditions. The unwanted niobium oxide phase in Figure 14 (a) was determined to most likely be the lithium poor fully oxidized phase, $LiNb_3O_4$, and so a lithium flux experiment was conducted to understand the role of lithium flux at this substrate temperature. Due to equipment constraints, the Li flux is controlled by power rather than temperature. In all previous experiments mentioned the Li bulk was held at a constant heating current of 6A, which corresponds to a beam equivalent pressure (BEP) on the order of 1.5×10^{-7} torr. In the present experiment the Li cell is taken to higher temperatures at currents of 6.25, 6.5, and 7A, shown in Figure 14. 7A corresponds to an approximate BEP of 3.5×10^{-7} torr. By increasing the Li flux the $LiNbO_2$ peak intensity increased and the auxiliary phases (unwanted niobium oxide and $LiNbO_3$) intensities decreased for both steps to 6.25 and 6.5 A Li heating current. The film grown at 7A Li heating current, however, showed almost no $LiNbO_2$ and is primarily an unwanted niobium oxide phase with a wide rocking curve (~2700 arcseconds) as well as $LiAlO_2$ which is also poorly oriented. In the 7A case however it was noticed that the sapphire backplate, which is exposed to a small amount of flux around the substrate, had a red deposit on it similar in color to previous $LiNbO_2$ films. Analyzing the film grown on this piece of sapphire shows a much

improved $LiNbO_2$ to other phases ratio, as shown in the diffractogram in Figure 15. This film also exhibits a best achieved 233 arcsecond omega rocking curve, indicating excellent crystalline uniformity. In this experiment the sapphire has no backside metal, but is in contact with the solid molybdenum back of the mounting block. The location is also far enough from the center of the mounting apparatus to have a more uniform temperature, which is theorized to be higher than the temperature at the center of the intended growth substrate. It should be noted, however, that the reduction in unwanted phases could be due to a smaller x-ray interaction volume than a shift in nucleation condition.

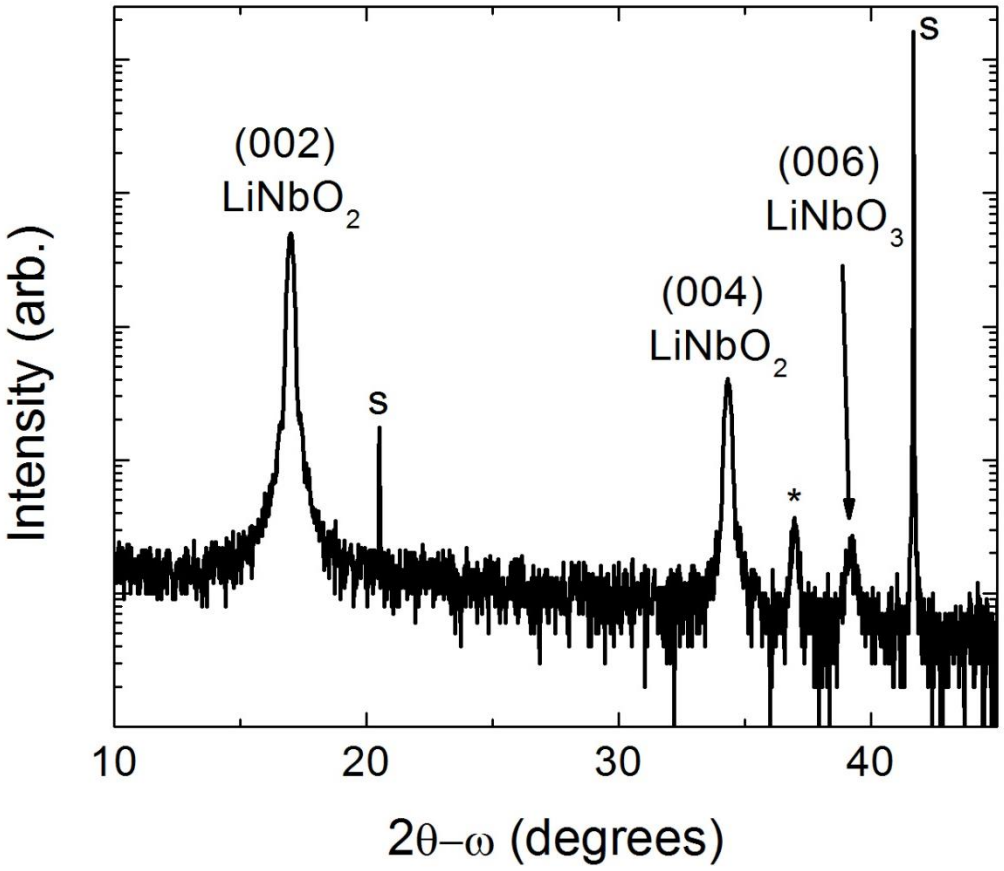

Figure 15. X-ray diffractogram of a film grown on the sapphire backplate with no backside metallization, with 7A Li current at ~1000 °C, representing the best yet condition for $LiNbO_2$ growth.

3.5 Tri-Lithium Niobate

The lithium rich state of fully oxidized niobium, tri-lithium niobate (Li_3NbO_4), has been grown using the same methods. Tri-lithium niobate is a lithium rich niobate existing towards Li_2O compositions greater than ~50% as shown on the Li_2O-Nb_2O_5 phase diagram [59, 60]. Tri-lithium niobite has been investigated as a Low Temperature Co-fired Ceramic (LTCC) and has shown promise as a dielectric with a permittivity of 15.8 and a quality factor, Q_f, of 55,009 GHz [61].

Using the methods described herein, high quality single crystal tri-lithium niobate has been grown using slightly lower growth temperatures than used for lithium niobite. At approximately 850 – 950°C the lithium rich environment preferentially nucleates to cubic tri-lithium niobite, which nucleates in the (222) direction along the hexagonal sapphire c-face with cubic lattice parameter a = 8.45 Å (bulk value 8.41 Å). The diffractogram of a characteristic Li_3NbO_4 film is shown in Figure 16, exhibiting Pendellösung fringes indicating a smooth surface and interface, and giving a film thickness of 75 nm for a 60 minute growth. The rocking curve for this reflection is shown in Figure 17 with a FWHM of 188 arcseconds indicating high crystalline quality.

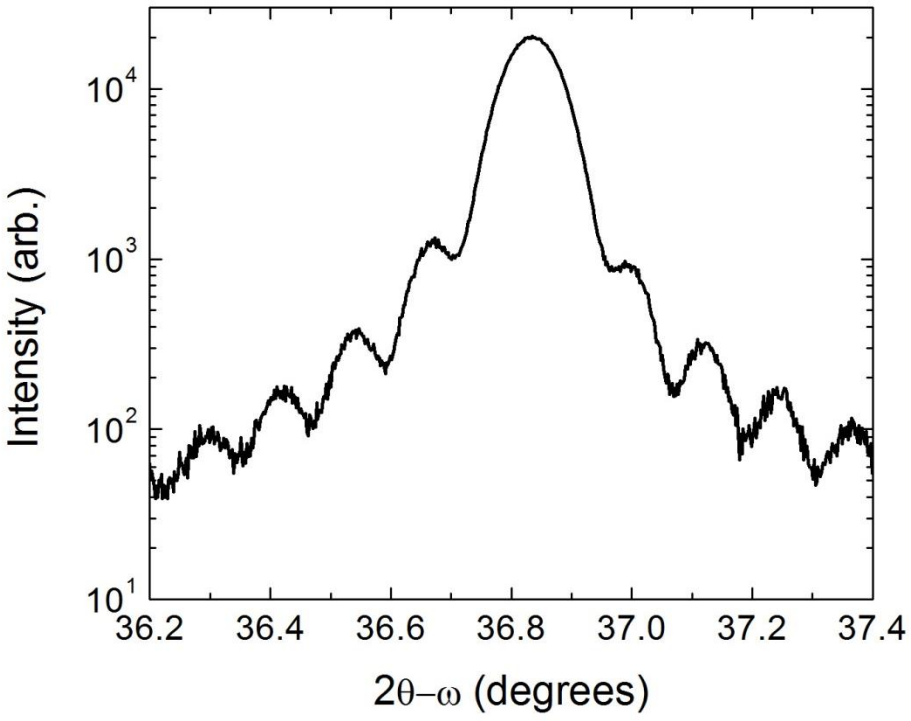

Figure 16. XRD symmetric scan around the Li_3NbO_4 (222) reflection showing Pendellösung fringes indicating a smooth 75nm thick film.

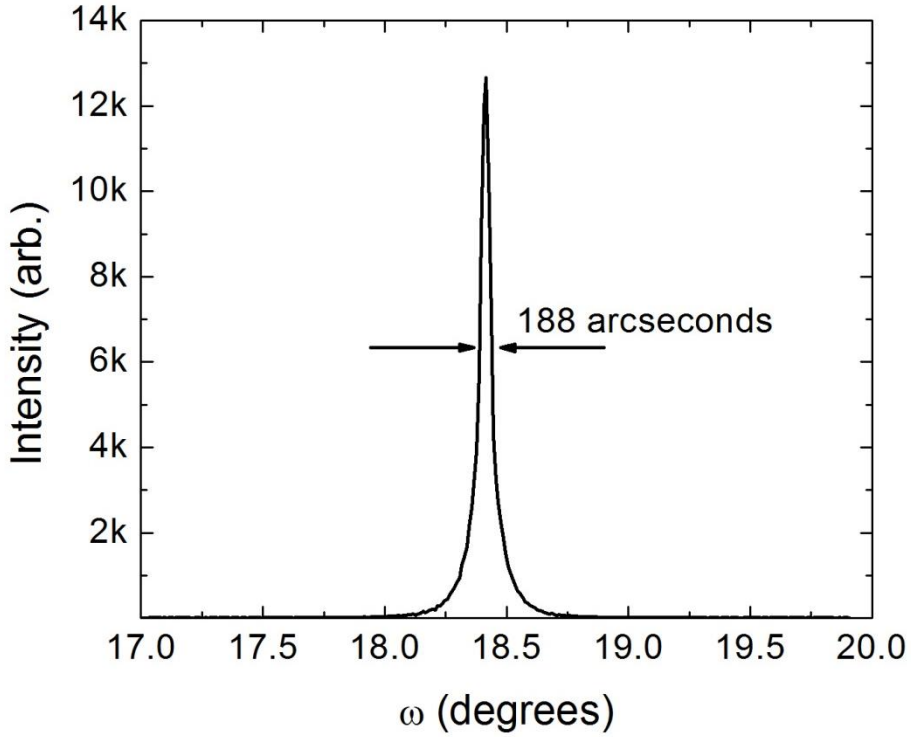

Figure 17. Rocking curve about the Li_3NbO_4 (222) reflection indicating a high degree of crystalline uniformity.

If grown at similar substrate temperatures in severely oxygen depleted environments, Li_3NbO_4 can be grown (100) oriented. Figure 18 shows the two-phase diffractogram of a film grown at low $LiClO_4$ fluxes in a severely lithium rich environment showing the (200), (400), and (600) reflections. Niobium (II) oxide, the suboxide with niobium in the +2 valence, is also present due to the oxygen starved atmosphere. While the results of this growth are interesting, further work to optimize the (100) oriented Li_3NbO_4 was not pursued.

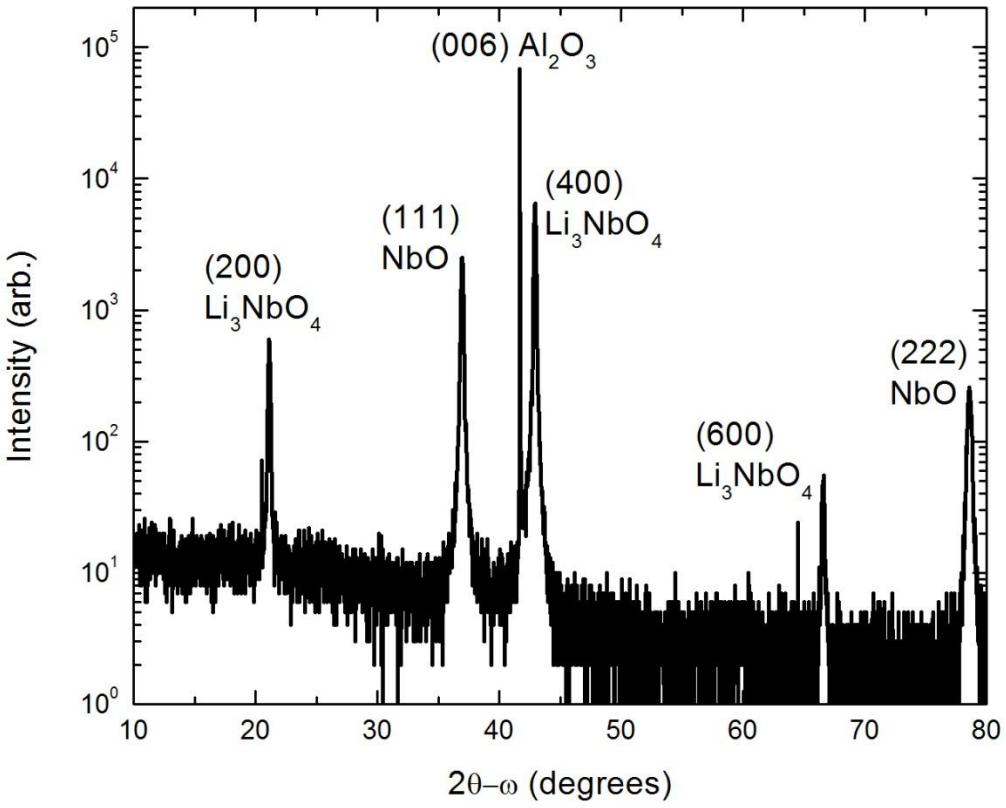

Figure 18. X-ray diffractogram showing a two phase film composed of (100) oriented Li_3NbO_4 and NbO. This result was obtained by oxygen deficient growth chemistry at high temperatures on an Al_2O_3 substrate.

3.6 Lithium Niobate

The growth of $LiNbO_3$ by the methods above has also been achieved. Figure 12 (d) shows the diffractogram of a film grown at 1000 °C exhibiting a large c-oriented $LiNbO_3$ (006) peak, as well as c-oriented $LiNbO_2$ and an unwanted niobium oxide phase. The $LiNbO_3$ phase has an omega rocking curve of 240 arcseconds indicating excellent crystalline uniformity. While the film is multi-phase by XRD analysis, visual analysis as shown in Figure 13 (b) indicates that the phases are physically separated on the wafer

with the $LiNbO_3$ in the center and the $LiNbO_2$ around the edges as previously discussed in section 3.4. The physical separation in these two films is likely due to a thermal gradient across the wafer. The center of the wafer is transparent under an optical microscope while the blue edges are not, indicating that the film in the center is $LiNbO_3$ and the edges are $LiNbO_2$. This theory is also supported by Raman Spectroscopy of the film which shows fluorescence at the edges of the wafer, but not at the center, for a 488 nm laser.

While no attempt to optimize the $LiNbO_3$ condition has been made, the same methodologies applied to optimizing $LiNbO_2$ can be applied to do so. Namely, sharper control over the Li:O flux ratio and temperature should allow single crystalline $LiNbO_3$ to be grown.

CONCLUSIONS AND FUTURE WORK

3.7 Summary and Contributions

In summary, $LiClO_4$ has been theorized, designed, and tested as a new oxygen source for MBE growth of oxide films. The material is found to decompose into a gas of both molecular and atomic oxygen by pressure and RGA studies, showing an atomic oxygen concentration for $LiClO_4$ much larger than the expected signal for cracked and doubly ionized O_2. The material begins decomposition at approximately 250 °C, with an Arrhenius flux relationship across the measured range of less than 400 °C to avoid exothermic decomposition.

A method for analyzing reaction rates has been demonstrated using *in situ* Auger Electron Spectroscopy, and $LiClO_4$ has been compared to 1 SCCM diffuse O_2 showing a comparable reaction rate at 4 times lower growth pressure, indicating the possibility for higher growth rates than are possible with O_2. The decomposition of $LiClO_4$ has been shown to be erratic and unstable by chamber pressure measurements and RGA partial pressure, and solutions are hypothesized for future studies on the material.

A new style of MBE effusion cell has also been presented, utilizing a two-zone heating system and aperture plate to resolve previous issues associated with secondary radiative heating from the substrate. The cell flux is shown to operate as expected, and is stable over time within the error range of the measurement tools.

Along with lithium, these two cells have been used to grow thin films of multiple niobium oxidation states. Films grown include pure BCC niobium, NbO, $LiNbO_2$, Li_3NbO_4, and $LiNbO_3$. The most important films are high quality $LiNbO_2$ which have been grown using the method outlined in this work, and the growth space has been

studied showing the preferential nucleation and growth of $LiNbO_2$ at high substrate temperatures. The best result for $LiNbO_2$ as measured by XRD rocking curve was 233 arcseconds, achieved at a substrate temperature of 1000 °C.

3.8 Future Work

Future work will continue the optimization of the $LiNbO_2$ and $LiNbO_3$ growth process by obtaining single phase material and optimizing those conditions for material quality, namely structure by XRD rocking curve, insulator resistance by electrometer, and memristance characterization by electrochemical impedance spectroscopy (EIS) and frequency dependent cyclical current-voltage (IV) measurements. All facilities needed to complete this work are available through the Institute for Electronics and Nanotechnology (IEN) and the Advanced Semiconuctor Technology Facility at the Georgia Institute of Technology.

REFERENCES

[1] S. Matsuda and A. Kato, "Titanium oxide based catalysts-a review," *Applied catalysis,* vol. 8, pp. 149-165, 1983.

[2] A. Sawa, "Resistive switching in transition metal oxides," *Materials today,* vol. 11, pp. 28-36, Jun 2008.

[3] S. D. Ha and S. Ramanathan, "Adaptive oxide electronics: A review," *Journal of Applied Physics,* vol. 110, p. 071101, Oct 1 2011.

[4] W. L. Calley, J. D. Greenlee, W. E. Henderson, J. Lowder, M. W. Moseley, W. A. Doolittle, *et al.*, "In situ Auger probe enabling epitaxy composition control of alloys by elemental surface analysis," *Journal of Vacuum Science & Technology B,* vol. 31, p. 03C126, May 2013.

[5] V. Eyert, "The metal-insulator transition of NbO_2: An embedded Peierls instability," *EPL (Europhysics Letters),* vol. 58, p. 851, 2002.

[6] T. Cardinal, E. Fargin, G. Le Flem, M. Couzi, L. Canioni, P. Segonds, *et al.*, "Non linear optical properties of some niobium (V) oxide glasses," *European journal of solid state and inorganic chemistry,* vol. 33, pp. 597-606, 1996.

[7] M. D. Pickett, G. Medeiros-Ribeiro, and R. S. Williams, "A scalable neuristor built with Mott memristors," *Nature materials,* vol. 12, pp. 114-117, Feb 2013.

[8] S. Li, X. Liu, S. K. Nandi, D. K. Venkatachalam, and R. G. Elliman, "High-endurance megahertz electrical self-oscillation in Ti/NbO_x bilayer structures," *Applied Physics Letters,* vol. 106, p. 212902, 2015.

[9] R. S. Weis and T. K. Gaylord, "Lithium niobate: Summary of physical properties and crystal structure," *Applied Physics A,* vol. 37, pp. 191-203, 1985/08/01 1985.

[10] J. C. Shank, M. B. Tellekamp, E. X. Zhang, W. G. Bennett, M. W. McCurdy, D. M. Fleetwood, *et al.*, "Self-Healing of Proton Damage in Lithium Niobite," *Nuclear Science, IEEE Transactions on,* vol. 62, pp. 542-547, 2015.

[11] J. D. Greenlee, W. Calley, W. Henderson, and W. A. Doolittle, "Halide based MBE of crystalline metals and oxides," *physica Status Solidi C Current Topics in Solid State Physics,* vol. 9, pp. 155-160, 2012.

[12] J. D. Greenlee, W. Calley, M. W. Moseley, and W. Doolittle, "Comparison of Interfacial and Bulk Ionic Motion in Analog Memristors," 2013.

[13] J. D. Greenlee, C. F. Petersburg, W. Laws Calley, C. Jaye, D. A. Fischer, F. M. Alamgir, *et al.*, "In-situ oxygen x-ray absorption spectroscopy investigation of the resistance modulation mechanism in $LiNbO_2$ memristors," *Applied Physics Letters,* vol. 100, pp. 182106-182106-4, 2012.

[14] J. D. Greenlee, J. C. Shank, M. Brooks Tellekamp, and W. Alan Doolittle, "Spatiotemporal drift-diffusion simulations of analog ionic memristors," *Journal of Applied Physics,* vol. 114, pp. 034504-034504-9, 2013.

[15] J. D. Greenlee, J. C. Shank, M. B. Tellekamp, Z. En Xia, B. Jinshun, D. M. Fleetwood, *et al.*, "Radiation Effects on $LiNbO_2$ Memristors for Neuromorphic Computing Applications," *Nuclear Science, IEEE Transactions on,* vol. 60, pp. 4555-4562, 2013.

[16] J. D. Greenlee, J. C. Shank, M. B. Tellekamp, B. Gunning, C. A. Fabien, and A. Doolittle, "Liquid Phase Electro-Epitaxy of Memristive $LiNbO_2$ Crystals," *Crystal Growth & Design,* 2014.

[17] J. C. Shank, M. B. Tellekamp, and W. A. Doolittle, "Evidence of ion intercalation mediated band structure modification and opto-ionic coupling in lithium niobite," *Journal of Applied Physics,* vol. 117, p. 035704, 2015.

[18] E. Moshopoulou, P. Bordet, and J. Capponi, "Superstructure and superconductivity in $Li_{1-x}NbO_2$ ($x\approx 0.7$) single crystals," *Physical Review B,* vol. 59, p. 9590, 1999.

[19] N. Kumada, S. Watauchi, I. Tanaka, and N. Kinomura, "Superconductivity of hydrogen inserted $LiNbO_2$," *Materials research bulletin,* vol. 35, pp. 1743-1746, 2000.

[20] M. J. Geselbracht, T. J. Richardson, and A. M. Stacy, "Superconductivity in the layered compound Li_xNbO_2," *Nature,* vol. 345, pp. 324-326, 05/24/print 1990.

[21] M. J. Geselbracht, A. M. Stacy, A. R. Garcia, B. G. Silbernagel, and G. H. Kwei, "Local environment and lithium ion mobility in $LiNbO_2$: inferences from structure, physical properties, and NMR," *Journal of Physical Chemistry* vol. 97, pp. 7102-7107, 1993.

[22] N. Kumada, S. Muramatu, F. Muto, N. Kinomura, S. Kikkawa, and M. Koizumi, "Topochemical reactions of Li_xNbO_2," *Journal of Solid State Chemistry,* vol. 73, pp. 33-39, 3// 1988.

[23] S. Chang, H. Park, A. Maazaz, and C. Delmas, "On the preparation of the $LiNbO_2$ and $NaNbO_2$ layer oxides by chemical and electrochemical ways-elaboration of the corresponding solid-solutions," *Comptes Rendus de L'Acadamie des Sciences Serie II,* vol. 308, pp. 475-478, 1989.

[24] A. Soukiassian, W. Tian, V. Vaithyanathan, J. Haeni, L. Chen, X. Xi, *et al.*, "Growth of nanoscale $BaTiO_3/SrTiO_3$ superlattices by molecular-beam epitaxy," *Journal of Materials Research,* vol. 23, pp. 1417-1432, 2008.

[25] R. Ramesh and N. A. Spaldin, "Multiferroics: progress and prospects in thin films," *Nat Mater,* vol. 6, pp. 21-9, Jan 2007.

[26] F. Gitmans, Z. Sitar, and P. Günter, "Growth of tantalum oxide and lithium tantalate thin films by molecular beam epitaxy," *Vacuum,* vol. 46, pp. 939-942, Aug-Oct 1995.

[27] W. A. Doolittle, A. Carver, W. Henderson, and W. L. Calley, "Molecular Beam Epitaxy of Lithium Niobate Multifunctional Materials Using a Chloride Refractory Metal Chemistry," *ECS Transactions,* vol. 2, pp. 103-114, 2006.

[28] D. Schlom, A. Marshall, J. Sizemore, Z. Chen, J. Eckstein, I. Bozovic, *et al.*, "Molecular beam epitaxial growth of layered Bi-Sr-Ca-Cu-O compounds," *Journal of crystal growth,* vol. 102, pp. 361-375, 1990.

[29] W. E. Henderson, W. Laws Calley, A. G. Carver, H. Chen, and W. Alan Doolittle, "A versatile metal-halide vapor chemistry for the epitaxial growth of metallic, insulating and semiconducting films," *Journal of Crystal Growth,* vol. 324, pp. 134-141, Jun 1 2011.

[30] A. Cho, "Film deposition by molecular-beam techniques," *Journal of Vacuum Science & Technology,* vol. 8, pp. S31-S38, 1971.

[31] A. Cho and J. Arthur, "Molecular beam epitaxy," *Progress in solid state chemistry,* vol. 10, pp. 157-191, 1975.
[32] B. Joyce, "Molecular beam epitaxy," *Reports on Progress in Physics,* vol. 48, p. 1637, 1985.
[33] A. Cho, "Morphology of epitaxial growth of GaAs by a molecular beam method: the observation of surface structures," *Journal of Applied Physics,* vol. 41, pp. 2780-2786, 1970.
[34] G. Biasiol and L. Sorba, "Molecular beam epitaxy: principles and applications," *Crystal growth of materials for energy production and energy-saving applications,* pp. 66-83, 2001.
[35] O. K. Wu and G. S. Kamath, "An overview of HgCdTe MBE technology," *Semiconductor Science and Technology,* vol. 6, p. C6, 1991.
[36] H. Morkoç, "III-Nitride semiconductor growth by MBE: Recent issues," *Journal of Materials Science: Materials in Electronics,* vol. 12, pp. 677-695, 2001.
[37] D. Schlom, J. Haeni, J. Lettieri, C. Theis, W. Tian, J. Jiang, *et al.*, "Oxide nano-engineering using MBE," *Materials Science and Engineering: B,* vol. 87, pp. 282-291, 2001.
[38] J. A. Peters, M. Klanchar, T. G. Hughes, and J. C. Mankin, "Means for heating and holding liquid lithium perchlorate for decomposition into lithium chloride and oxygen," US5376352A, 1994.
[39] M. M. Markowitz, D. A. Boryta, and H. Stewart Jr, "Lithium Perchlorate Oxygen Candle. Pyrochemical Source of Pure Oxygen," *Industrial & Engineering Chemistry Product Research and Development,* vol. 3, pp. 321-330, 1964.
[40] J. P. Simmons and C. D. L. Ropp, "THE SYSTEM LITHIUM PERCHLORATE—WATER," *Journal of the American Chemical Society,* vol. 50, pp. 1650-1653, 1928/06/01 1928.
[41] M. M. Markowitz and D. A. Boryta, "The decomposition kinetics of lithium perchlorate," *Journal of Physical Chemistry* vol. 65, pp. 1419-1424, 1961.
[42] K. H. Stern, *High temperature properties and thermal decomposition of inorganic salts with oxyanions*: CRC press, 2000.
[43] P. G. Staib, "In situ real time Auger analyses during oxides and alloy growth using a new spectrometer design," *Journal of Vacuum Science & Technology B,* vol. 29, p. 03C125, May 2011.
[44] J. M. Sanz and S. Hofmann, "Auger electron spectroscopy and X-ray photoelectron spectroscopy studies of the oxidation of polycrystalline tantalum and niobium at room temperature and low oxygen pressures," *Journal of the Less Common Metals,* vol. 92, pp. 317-327, 8// 1983.
[45] M. M. Markowitz and D. A. Boryta, "RETARDATION OF THE THERMAL DECOMPOSITION OF LITHIUM PERCHLORATE," *Journal of Physical Chemistry* vol. 66, pp. 358-358, 1962.
[46] D. Finnemore, T. Stromberg, and C. Swenson, "Superconducting properties of high-purity niobium," *Physical Review,* vol. 149, p. 231, 1966.
[47] J. Halbritter, "On the oxidation and on the superconductivity of niobium," *Applied Physics A,* vol. 43, pp. 1-28, 1987.
[48] A. Wildes, J. Mayer, and K. Theis-Bröhl, "The growth and structure of epitaxial niobium on sapphire," *Thin solid films,* vol. 401, pp. 7-34, 2001.

[49] G. Chandrashekhar, J. Moyo, and J. Honig, "Electrical resistivity of NbO," *Journal of Solid State Chemistry,* vol. 2, pp. 528-530, 1970.
[50] W. W. Schulz and R. M. Wentzcovitch, "Electronic band structure and bonding in Nb_3O_3," *Physical Review B: Condensed Matter* vol. 48, p. 16986, 1993.
[51] A. F. McDowell, D. M. Snyderman, M. S. Conradi, B. G. Silbernagel, and A. M. Stacy, "Cross relaxation and atomic motion in $LiNbO_2$," *Physical Review B,* vol. 50, pp. 15764-15774, 12/01/ 1994.
[52] D. G. Kellerman, V. S. Gorshkov, A. P. Tyutyunnik, V. G. Zubkov, V. A. Perelyaev, T. V. D'yachkova, *et al.*, "Synthesis, superconductiong properties, and electronic structure of Li_xNbO_2," *Superconductivity: Physics, Chemistry, Technology,* vol. 5, pp. 2035-2042, 1992.
[53] J. K. Burdett and T. Hughbanks, "Aspects of metal-metal bonding in early-transition-metal dioxides," *Inorganic Chemistry,* vol. 24, pp. 1741-1750, 1985.
[54] V. Cherkashenko, M. Korotin, V. Anisimov, V. Shumilov, V. Galakhov, D. Kellerman, *et al.*, "X-ray spectra and electronic structure of Li_xNbO_2 superconductor and other niobium oxide compounds," *Zeitschrift für Physik B Condensed Matter,* vol. 93, pp. 417-424, 1994.
[55] D. Novikov, V. Gubanov, V. Zubkov, and A. Freeman, "Electronic structure and electron-phonon interactions in layered Li_xNbO_2 and Na_xNbO_2," *Physical Review B,* vol. 49, pp. 15830 - 15835, 1994.
[56] S. Turzhevsky, D. Novikov, V. Gubanov, and A. Freeman, "Electronic structure and crystal chemistry of niobium oxide phases," *Physical Review B,* vol. 50, pp. 3200 - 3208, 1994.
[57] E. R. Ylvisaker and W. E. Pickett, "First-principles study of the electronic and vibrational properties of Li Nb O 2," *Physical Review B,* vol. 74, p. 075104, 2006.
[58] E. R. Dobrovinskaya, L. A. Lytvynov, and V. Pishchik, *Sapphire: material, manufacturing, applications*: Springer Science & Business Media, 2009.
[59] R. Roth, H. Parker, W. Brower, and J. Waring, "Phase equilibria, crystal chemistry and crystal growth of alkali oxide-metal oxide systems. Fast ion transport in solids," *Ed. W. Van Gool, North Holland,* vol. 217, 1973.
[60] A. Reisman and F. Holtzberg, "Heterogeneous equilibria in the systems Li_2O-, Ag_2O-Nb_2O_5 and oxide-models," *Journal of the American Chemical Society,* vol. 80, pp. 6503-6507, 1958.
[61] D. Zhou, H. Wang, L. X. Pang, X. Yao, and X. G. Wu, "Microwave dielectric characterization of a Li_3NbO_4 ceramic and its chemical compatibility with silver," *Journal of the American Ceramic Society,* vol. 91, pp. 4115-4117, 2008.